Science Advances

AAAS

advances.sciencemag.org/cgi/content/full/1/11/e1500911/DC1

Supplementary Materials for

Mechanisms of murine cerebral malaria: Multimodal imaging of altered cerebral metabolism and protein oxidation at hemorrhage sites

Mark J. Hackett, Jade B. Aitken, Fatima El-Assaad, James A. McQuillan, Elizabeth A. Carter, Helen J. Ball, Mark J. Tobin, David Paterson, Martin D. de Jonge, Rainer Siegele, David D. Cohen, Stefan Vogt, Georges E. Grau, Nicholas H. Hunt, Peter A. Lay

Published 18 December 2015, *Sci. Adv.* **1**, e1500911 (2015)
DOI: 10.1126/sciadv.1500911

The PDF file includes:

Supplementary Information

Supplementary Text

Animal Models

In order to investigate the biochemical mechanisms of CM, several mouse models that closely reflect the human condition are traditionally employed *(13,73).* Infection with *Plasmodium berghei* ANKA (PbA), experimental cerebral malaria (ECM), reflects human CM. Infection with *Plasmodium berghei* K173 (PbK) infections resembles human malaria without cerebral complications. The latter may result in mild malaria anaemia (MMA) or, in the later stages of infection, produce severe malaria anaemia (SMA), a complication without cerebral involvement and with terminal illness *(61).* These animal models enabled cerebral biochemical alterations associated with ECM to be compared against three sets of controls: MMA (no terminal illness, no cerebral complications, circulating parasite levels are the same as CM, parasitaemia ~10 %); SMA (terminal illness, no cerebral complications, circulating parasitaemia > 50 %); sham-injected control animals (no terminal illness, no cerebral complications, no circulating parasites). Such comparisons of the brains of ECM mice with those from each control group allowed discrimination among the biochemical changes that were specific to the cerebral condition and those that were a generic response to parasite infection or generically related to terminal illness.

It is important to note that micro-hemorrhage was only associated with ECM, and not the MMA or SMA animal models. Therefore, elemental mapping of Fe distribution in the cerebellum was only performed for ECM and sham mice used in this study.

Histological Features of ECM

The classical histological features of ECM, such as immune cell sequestration, blood-brain-barrier (BBB) compromise, micro-hemorrhage, were characterized by hematoxylin and eosin staining, and immuno-histochemical staining of fibrinogen with a hematoxylin counterstain. As can be seen in Figure 1 and 2 of the main text, darker staining that indicated the presence of the plasma protein fibrinogen in the brain parenchyma of mice with ECM (relative to sham-injected control mice), confirmed that there was increased BBB permeability to protein. In

addition, the hematoxylin counterstain revealed numerous nuclei sequestered within the vessel of the ECM diseased mice, which indicated the presence of sequestered leukocytes.

Validation of Spectroscopic Markers of Anaerobic Brain Metabolism and Peroxidative Stress for FTIRM: Analysis of Relative Concentration from Second-Derivatives of the FTIR Spectra

Analysis of second-derivative band intensity provided significant advantages for determination of the relative molecular concentration compared to band area in raw spectra, as the second derivatives of the spectra were less affected by baseline distortions, and contained superior band resolution to separate overlapping bands. However, second-derivative band intensity is a measure of the rate of change of the slope as opposed to a direct measurement of concentration. Therefore, direct analysis of second-derivative band intensities has limitations as they are proportional to concentration only when band width at half-height is conserved. This complicated determinations of absolute concentrations from the analysis of second-derivatives of the spectra. However, the method has been used extensively, and is well-validated in the field of biological spectroscopy for identification of relative changes in molecular concentration *(28,36,37,74).*

Validation of Spectroscopic Markers of Anaerobic Brain Metabolism and Peroxidative Stress for FTIRM: Validation of FTIR Spectroscopic Marker Bands of Lactate

The spectroscopic regions at which lactate absorbs in mid infrared spectra were determined via addition of lactate to brain homogenates. As reported by others, characteristic and pronounced absorbance was observed due to the ν(C–O) band at ~1127 cm^{-1} (Figure S1) *(28,39,75-78).* In dehydrated films of biological fluids, or in air-dried tissue sections, we observed this band at 1127 cm^{-1}, in agreement with the published literature *(77)*, but in aqueous solution (i.e., Figure S1A) we observed a red shift for this band, to 1125 cm^{-1}, most likely due to hydrogen bonding in solution, which was observed for other biological molecules *(79)*. In order to validate that the absorbance at this region in the FTIR spectra collected from brain tissue corresponded to the endogenous lactate concentration, FTIR spectra were collected from brain homogenates prepared from unadulterated brain tissue, after the addition of lactate, and after the addition of lactate dehydrogenase (which metabolises lactate to pyruvate). As shown in the Figure S1A, addition of lactate to the sample resulted in increased second-derivative band

intensity, and a decrease in the spectral signal over time was observed following addition of lactate dehydrogenase. To further establish that the band at 1127 cm^{-1} was a spectroscopic marker that can be used for semi-quantitative analysis of the relative lactate concentration in brain tissue, a linear correlation was demonstrated between the second-derivative band intensity at 1127 cm^{-1} and the known lactate concentration (determined from enzymatic assay) of a series of brain homogenates (Figure S1B-D).

Validation of Spectroscopic Markers of Anaerobic Brain Metabolism and Peroxidative Stress for FTIRM: Validation of Spectroscopic Marker Bands of Aggregated β-Sheet Proteins, as a Direct Indicator of Protein Oxidation for FTIRM

Numerous studies have used FTIR spectroscopy to study the location of β-sheet proteins in biological samples, based on characteristic absorbance of the amide 1 band between 1620-1640 cm^{-1} *(34,36-38,80-87)*. However, few investigations have sought to identify and validate the specific location of a spectroscopic marker for high molecular weight β-sheet aggregates in brain tissue, a direct product of protein oxidation *(23)*. To determine the spectroscopic alterations that occurred due to protein oxidation, FTIR spectra were collected from brain homogenates before and after the addition of Fe(II) ($FeSO_4$), or Fe(II) ($FeSO_4$) plus the Fe chelator Desferal (Figure S2). A significant decrease in band intensity was observed at 1656 cm^{-1} (assigned to α-helix proteins) and 1640 cm^{-1} and a significant increase in band intensity at 1625 cm^{-1} (assigned to aggregated β-sheet proteins) was observed following the addition of Fe(II). The increase in second-derivative band intensity at 1625 cm^{-1} was partially mitigated by the co-addition of the Fe chelator (Figure S2). These results were indicative of the production of high molecular weight β-sheet protein aggregates, which are known to be formed as a consequence of protein oxidation *(23)*.

Identification of Tissue Regions and Determination of Regions of Interests.

Determination of the specific tissue layers of the cerebellum from histology (H&E) is trivial, and as can be seen from Figure S3, characteristic lipid levels were observed within the molecular, granular, and inner white matter layers of the cerebellum. This allowed simple overlay of FTIRM images of the lipid distribution with histology to determine regions of interest that corresponded to those layers. This process has been used successfully and published

numerous times *(28-31,36,46)* The location of micro-hemorrhage in the inner white matter was also straightforward due to the significant loss of lipid from an otherwise lipid rich region and the eosinophilic nature of the hemorrhaged tissue.

Multivariate Analysis

In addition to univariate analysis, a multivariate analytical approach was employed, similar to that used by others *(88)*. Hierarchical cluster analysis (HCA) was used to cluster spectra within each image into four groups. For cerebellum tissue from ECM mice, these four clusters also correlated with the location of the molecular layer, granular layer, inner white matter, and hemorrhaged tissue (Figure S4). For control animals (Sham, MMA, SMA), the three clusters were found to correlate to the molecular layer, granular layer, and inner white matter. The fourth cluster typically correlated to the interface of the granular layer and inner white matter (Figure S4).

The average spectrum was extracted from each cluster, for each animal (n = 5), and used for principal component analysis to identify the spectral locations that allowed discrimination among experimental groups. Note, for control animals, both the cluster that corresponded to the inner white matter, and also the cluster at the interface of white matter and the granular layer, were assigned to the "white matter" for PCA.

Principal Component Analysis of FTIR Spectra

Figure S5 shows the scores and loadings plots from multivariate, principal component analysis (PCA) of the data. The second derivatives of the averaged spectra for each tissue layer of the cerebellum (determined from HCA) were used as the input spectra for PCA. Three separate principal component analyses were performed: Figure S5A,B – lipid carbonyl and amide I region of white matter (1760-1600 cm^{-1}); Figure S5C,D – carbohydrate and organophosphate region of white matter (1260-950 cm^{-1}); Figure S5E,F – lipid carbonyl and amide I region of granular layer (1760-1600 cm^{-1}). The four-cluster HCA described two clusters for white matter (either two non-hemorrhaged regions for control animals, or one hemorrhaged and one non-hemorrhaged region for CM mice). The second derivatives of the averaged spectra for both clusters for the white matter were used for PCA (i.e., n = 5 animals resulted in ten spectra for white matter, and five spectra each for the granular and molecular layers).

As can be seen in the score plots in Figure S5A, spectra from hemorrhaged white matter of mice with ECM were separated along principal component 1 (PC1), and displayed more positive scores than those from the non-hemorrhaged white matter of these animals and the spectra from control mice (Sham, MMA, SMA). The strong negative loadings observed in Figure S5B near the position of the protein α-helix band (1656 cm^{-1}) and aggregated protein β-sheet band (1622 cm^{-1}) suggested that there was increased second-derivative band intensity at these regions, and implied elevated content of proteins with α-helix and aggregated β-sheet secondary structure in hemorrhaged white matter tissue in ECM mice. Further, a strong positive loading was observed at the location of the lipid carbonyl band (γ) at 1742 cm^{-1}, which indicated reduced second-derivative band intensity and lipid loss in the hemorrhaged white matter tissue of the ECM mice. These results are in direct agreement with those obtained from the univariate analysis.

Analysis of the spectral range 1260-950 cm^{-1} also indicated lipid loss within the hemorrhaged white matter of mice with ECM. As can be seen in Figure S5C, PC1 separated spectra from hemorrhaged white matter; these spectra displayed more positive scores. The PC1 loadings plot presented in Figure S5D revealed strong positive loadings for bands at 1244, 1084, 1066, and 970 cm^{-1} (γ_1, γ_2, γ_3, γ_4, respectively), which indicated reduced second-derivative intensity of characteristic phospholipid absorption bands $\nu_{as}(PO_2^-)$, $\nu_s(PO_2^-)$, ν(C–O), and ν(P–O–C), respectively. As the univariate analysis demonstrated increased lactate in the hemorrhaged white matter of ECM mice, a strong negative loading would be expected at 1127 cm^{-1}, and indeed this was observed (indicated by δ in the Figure S5D). The loadings plot also revealed strong negative loadings at 1107 and 1000 cm^{-1}. At present, the molecular identities of the species that correspond to these bands in the loadings remain unknown, but will be investigated further.

A substantial difference was observed between the loadings plot for PCA analysis of the lipid carbonyl and amide I region of the granular layer compared to the white matter. As hemorrhage was not present in the granular layer, substantial lipid loss or elevated α-helix protein content (from serum proteins) were not expected and, indeed, neither a strong positive loading at 1742 cm^{-1} nor a strong negative loading at 1656 cm^{-1} were observed. Univariate analysis indicated protein oxidation within the granular layer, which resulted in decreased content of α-helix proteins, and increased content of aggregated β-sheet protein. Therefore, the results from PCA

analysis, which revealed strong positive loadings at 1656 cm^{-1}, and strong negative loadings at 1625 cm^{-1}, are in strong agreement with the results from univariate analysis.

Determination of Characteristic Spectral Features due to Electric Field Standing Wave Interference and Mie Scattering

It has been demonstrated that FTIR spectra collected from biological samples, in either transmission or "transflection" mode, do not necessarily represent the true absorbance spectrum, but often contain contributions from Mie scattering, or electric field standing wave (EFSW) interference (particularly if measurements were performed in a transflection geometry) *(89-93)*. These processes result in characteristic shifts of the amide I band, which can result in mis-interpretation of the data, and incorrect assignment to variation in the relative absorbance by α-helix and β-sheet proteins. To determine the nature of the spectroscopic features in cerebellum tissue, a preliminary experiment was performed, in transflection geometry. As can be seen in Figure S6, the characteristic sloping baseline and "derivative" appearance in the amide I region in raw spectra, and a shift in the position of second-derivative band minima across the amide I region, were observed in spectra collected at the interface of the white matter and granular layer. It is important to note that all scientific conclusions made in this study are drawn from spectra collected in transmission mode, which greatly reduced the possibility for misinterpretation of the spectral data, and all spectra displayed characteristic second-derivative band minima (i.e., α-helix at 1656 cm^{-1}) that were not observed to shift. Therefore, it is highly unlikely that the results and scientific conclusions drawn from this investigation have been affected by misinterpretation of spectra affected by EFSW or Mie scattering.

Preliminary Investigation of Fe Distribution in Healthy and Hemorrhaged Vasculature

As an initial investigation of the quantification of Fe in sham and ECM mouse brain microvessels, preliminary elemental mapping experiments were performed with SR-XRF and PIXE to demonstrate the ability of these methods to study healthy and hemorrhaged cerebral blood microvessels. Identification of the location of vessels with XRF has been previously reported at coarser spatial resolution *(94,95)*, and as can be seen in Figure S7, K, Ca, and Fe elemental maps highlight the location of vascular walls with the highest relative Fe concentration observed on the inside of the vessel wall.

In Figure S8, an example of Fe increase in the brain parenchyma is visualised through a line map cross section of a hemorrhaged vessel in an ECM mouse.

Supplementary Figures

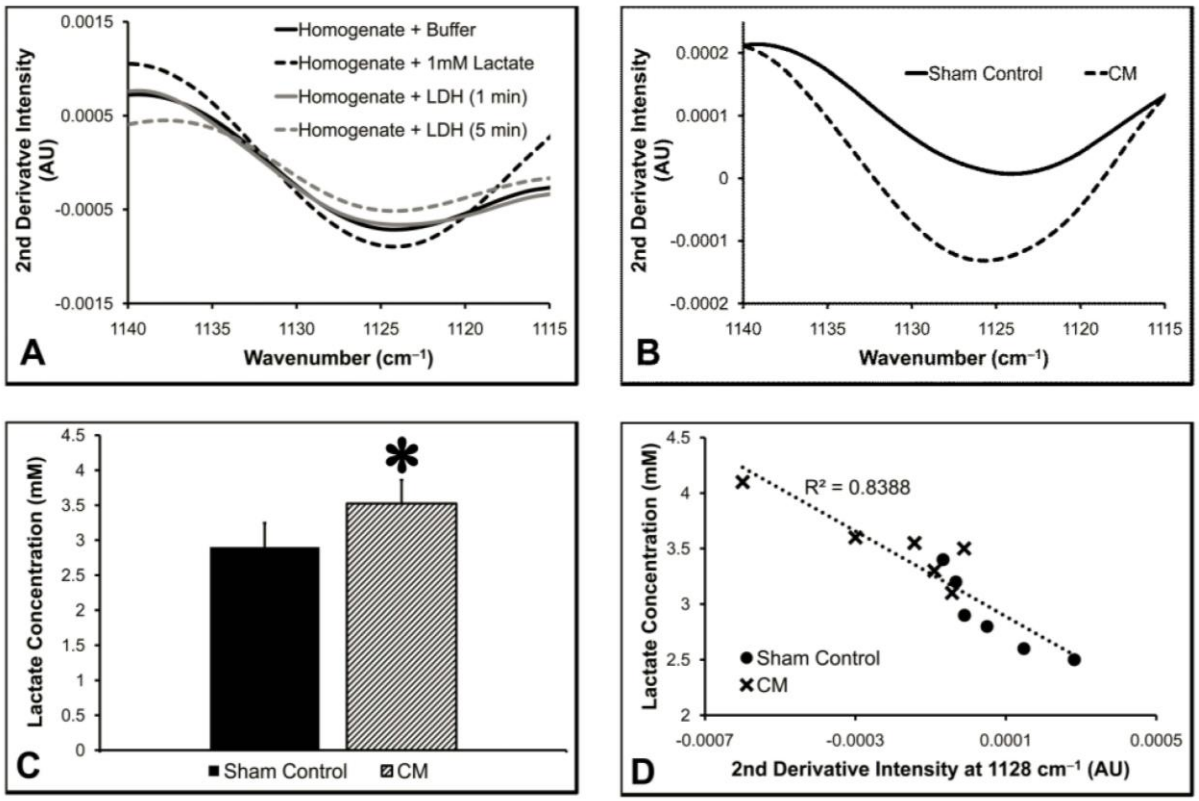

Figure S1: Validation of second-derivative band intensity at 1127 cm^{-1} in the FTIR spectra as a marker for relative lactate concentration. (**A**) Increased second-derivative band intensity observed following addition of lactate to brain homogenates, and a time dependent decrease observed following the addition of lactate dehydrogenase. (**B**) FTIR spectra from bulk brain homogenates demonstrated increased second-derivative band intensity at 1127 cm^{-1} in mice with CM relative to control mice, which supported (**C**) the increase in bulk lactate revealed from biochemical assay. The asterisk denotes significant difference. (**D**) A linear correlation was observed between second-derivative band intensity at 1127 cm^{-1} in FTIR spectra collected from bulk brain homogenates and the lactate concentration determined from enzymatic assay of the same homogenates.

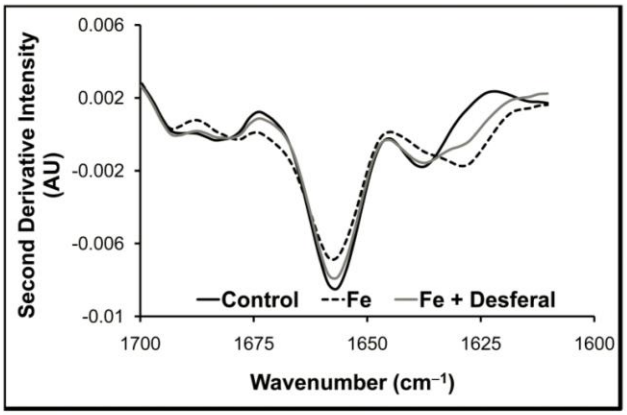

Figure S2: Validation of second-derivative band intensity at 1627 cm^{-1} in the FTIR spectra as a marker for relative concentration of aggregated β sheet proteins and, therefore, protein oxidation. Spectra were collected from brain homogenates without chemical modification, and after the addition of Fe(II), or Fe(II) with the Fe chelator Desferal.

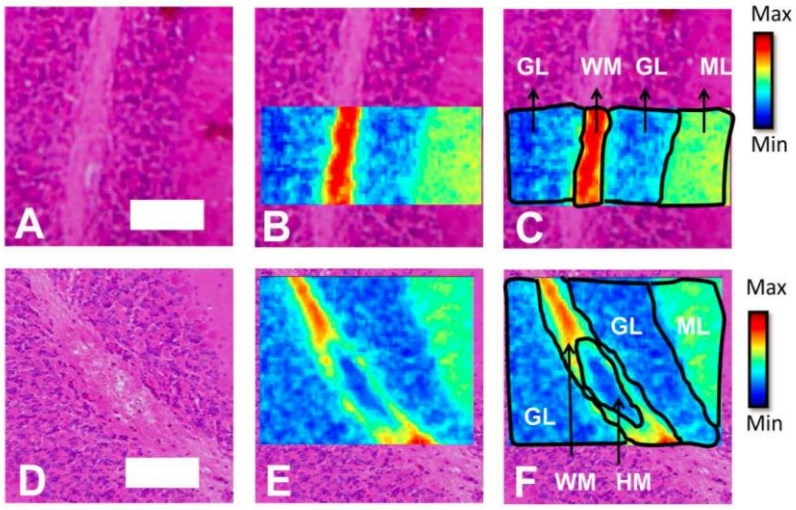

Figure S3: Correlation of FTIR maps of lipid distribution with H&E histology. Representative example of H&E histology from control (**A**) and CM mouse (**D**) cerebellum tissue, FTIR images of lipid distribution determined from second-derivative band intensity at 1742 cm^{-1} (**B, E**), and the regions of interest (**C, F**) drawn to determine the average spectra for molecular layer (ML), granular layer (GL) white matter (WM) and hemorrhaged white matter (HM) tissue.

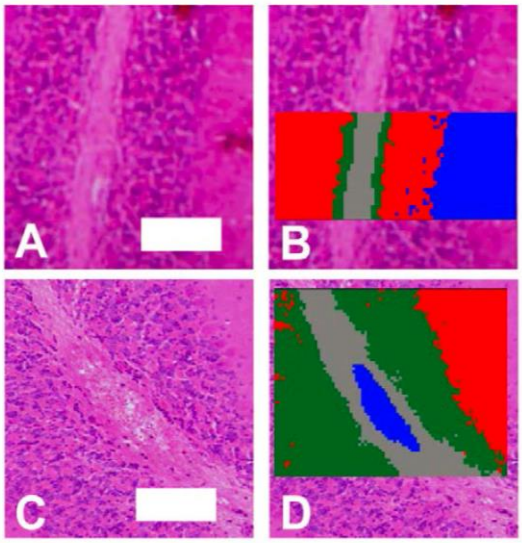

Figure S4: HCA analysis of FTIR maps distinguishes four distinct regions: the molecular layer, granular layer, inner white matter, and hemorrhaged white matter. Representative examples of a four group HCA analysis of FTIR images of cerebellum tissue from control (**A, B**) and CM (**C, D**) mice. In control tissue HCA analysis identified the molecular layer (blue), granular layer (red) and inner white matter (two clusters, green and grey). In CM mouse tissue, HCA identified the molecular layer (red) granular layer (green), inner white matter (grey) and hemorrhaged white matter (blue).

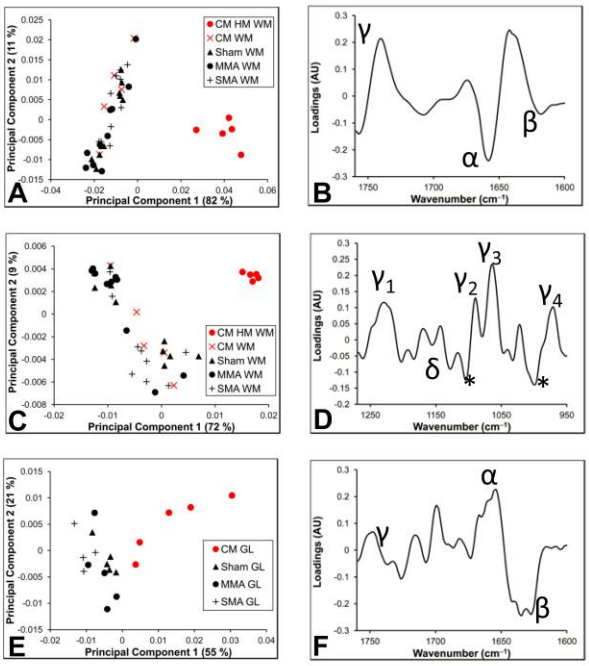

Figure S5: Principal components analysis of the average spectra for tissue layers determined from the HCA. (**A, C, E**) score plots (**B, D, F**) loadings plots. (**A,B**) White matter, spectral range 1760 -1600 cm^{-1}. (**C,D**) White matter spectral range 1260-950 cm^{-1}. (**E,F**) Granular layer, spectral range 1760-1600 cm^{-1}. Spectral positions identified with symbols: 1656 (α) 1625 (β) 1127 (δ) 1742 λ 1242 (λ_1) 1085 (λ_2) 1066 (λ_3) 970 (λ_4) cm^{-1}. Asterisks (*) designate the positions of bands at1107 and 1000 cm^{-1}.

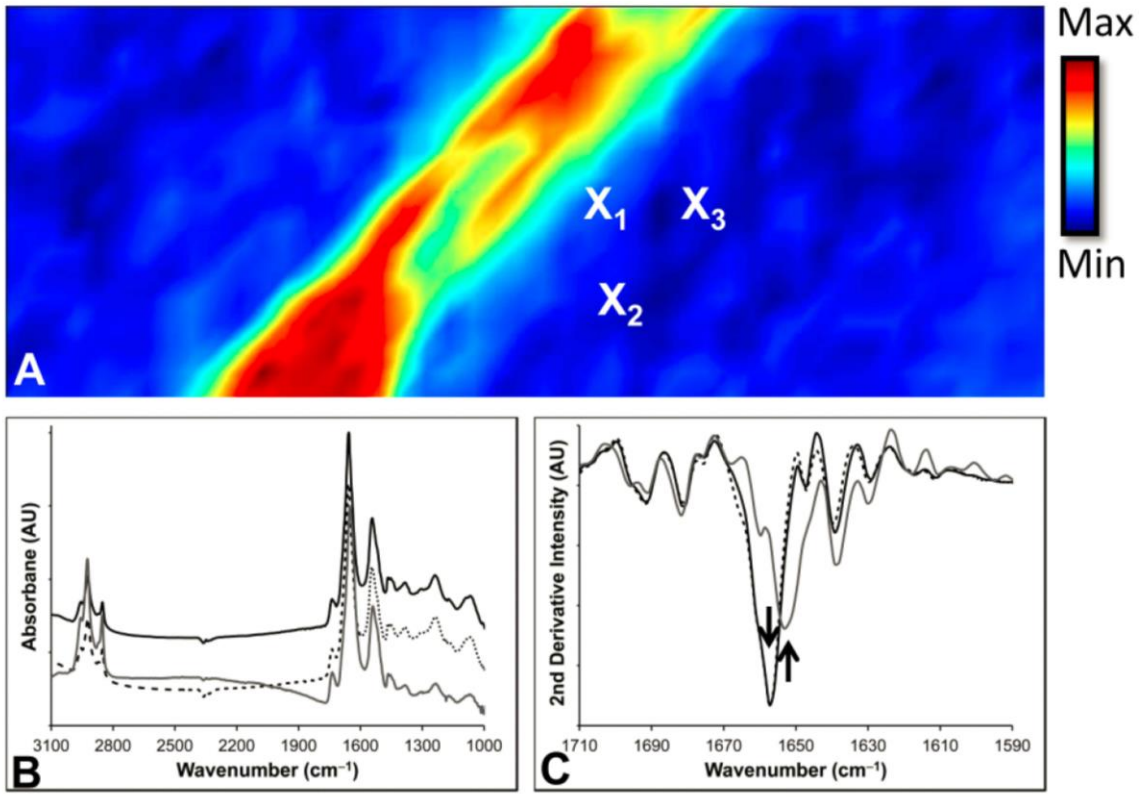

Figure S6: Synchrotron radiation–based (SR) FTIR mapping of cerebellum tissue to identify Mie scattering and electric field standing wave spectra features. (**A**) Lipid distribution in cerebellar white matter and granular layer (second-derivative band intensity 1742 cm^{-1}. (**B**) Raw spectra taken from position X1-3, and (**C**) second-derivatives of spectra from position X1-3. Spectra at the border of white matter and granular layer showed features characteristic of scattering, sloping baseline in raw spectra, and shift of the position of the dominant band in the second-derivatives of the spectra.

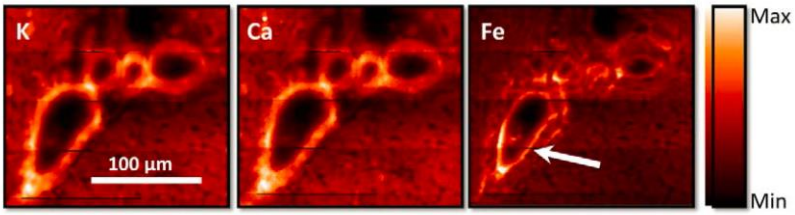

Figure S7: SR x-ray fluorescence elemental maps (2-µm step size) of healthy cerebellum blood vessels, showing location of Fe (white arrow) within the wall of the blood vessel.

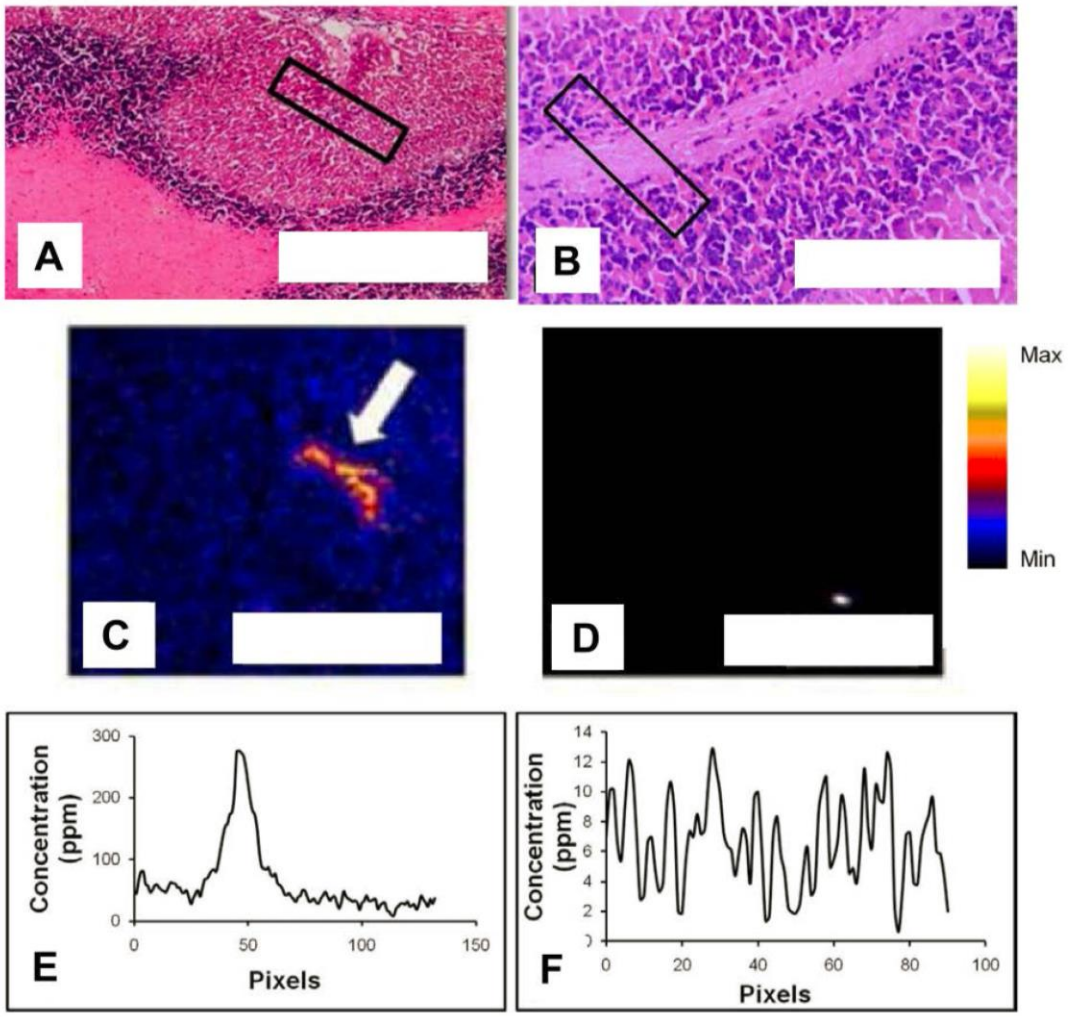

Figure S8: PIXE elemental maps of healthy and hemorrhaged cerebellum blood vessels. (**A, B**) H&E histology of hemorrhaged (**A**) and healthy (**B**) tissue. (**C, D**) Fe elemental maps of hemorrhaged and healthy tissue. (**E, F**) Line maps through vessel crossed section of hemorrhaged and healthy tissue. Scale Bar in A = 200 µm, B = 100 µm, C & D = 50 µm.

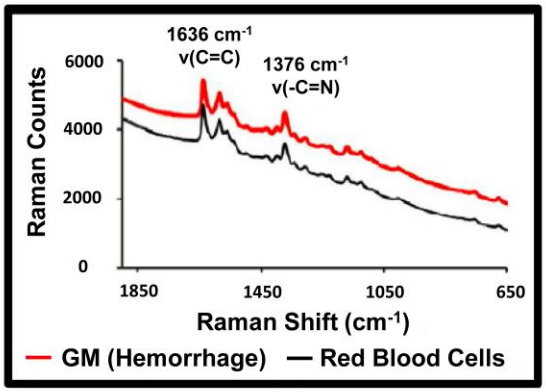

Figure S9: Resonance Raman spectra (514-nm excitation) collected from hemorrhaged tissue and dried red blood cells, showing characteristic enhanced intensity of hemoglobin bands.